Theoretical Comparison of Optical and Photothermal Properties of Near-Infrared Colloidal Plasmonic Nanoparticles

Kai Liu[1], Xiaozheng Xue[2], and Edward P. Furlani[1,2,*]

[1]Dept. of Electrical Engineering, University at Buffalo SUNY, NY 14260
[2]Dept. of Chemical and Biological Engineering, University at Buffalo SUNY, NY 14260
[*]efurlani@buffalo.edu

ABSTRACT

We study optical and photothermal properties of near-infrared absorbing colloidal plasmonic nanostructures that are of interest for biomedical theranostics: SiO2@Au core-shell particles, Au nanocages and Au nanorods. We investigate the absorption spectra and field enhancement of the structures as a function of their dimensions and orientation with respect to the incident field polarization. Computational models are also used to explore the transient thermal response of the particles. The modeling approach is well suited for the rational design of novel plasmon-assisted photothermal applications.

Keywords: Plasmonic nanoparticles, photothermal therapy, nanoframe, nanocage, nanorod, LSPR, plasmon-enhanced photothermal transduction, plasmon-enhanced theranostics, LSPR local field enhance-ment, plasmonic hot spot.

1 INTRODUCTON

In this presentation we use a combination of 3D photonic and thermodynamic computational models to study and compare the plasmonic and photothermal behavior of three distinct nanostructures that are of interest for a variety of applications including biomedical theranostics: SiO_2@Au core-shell particles, Au nanorods and Au nanocages as shown in **Figure 1**. Full-wave field analysis is used to predict the absorption spectra and field enhancement of these structures [1], whike computational thermodyna*m*ic models are used to explore their transient thermal response [2]. Our analysis shows that while the LSPR of all the structures can be tuned to the NIR, there are significant differences in their optical and thermal response that impact their selection for colloidal applications. The photonic analysis demonstrates that the photothermal conversion efficiency is highest for particles that have a high degree of rotational symmetry, i.e. the SiO_2@Au and nanocage structures. The heating efficiency is a complex function of multiple factors including the gold content of a particle and the degree to which it support LSPR-enhanced current to promote Joule heating. The thermal analysis elucidates fundamental mechanisms that govern the thermal diffusion in and around the particles. The multiphysics modeling approach used for this analysis can be adapted to plasmonic nanomaterials of arbitrary shapes, sizes and material constituents. It provides fundamental understanding of underlying photothermal mechanisms and enables the rational design of novel plasmon-assisted photothermal applications.

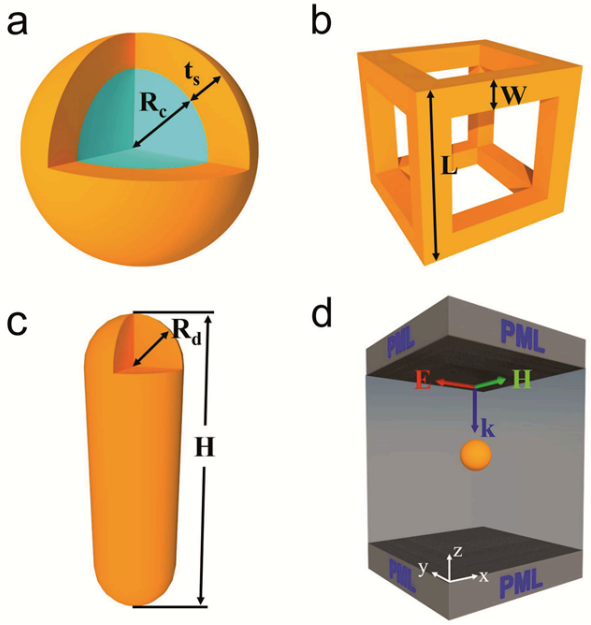

Figure 1. Plasmonic nanostructures and the computational model: (a) SiO_2@Au core-shell particles, (b) Au nanocages, (c) Au nanorods. (d) Computational domain showing the polarization and propagation direction of the incident field.

2 PHONTONICANALYSIS

We use 3D full-wave computational models to study the NIR plasmonic behavior of the three nanostructures shown in **Figure 1**. The core-shell particles consist of a silica (SiO_2) core with a radius R_c and a gold shell with a thickness t_s as shown in **Figure 1a**. The Au nanocages are cubic with twelve frame elements in the form of square Au nanowires (**Figure 1b**). The nanocage geometry is defined by its length L, which defines the size of the cube, the width W that defines the cross-sectional area of the nanowire, and the aspect ratio $R=L/W$. In the literature, this structure is also referred to a nanoframe. The nanorod geometry, shown in **Figure 1c,** consists of a cylindrical body of radius R_d

with hemispherical dome-shaped caps at either end. The total length of the nanorod is *H*.

We compare the optical properties of the nanostructures using the finite element (FE)-based Radio Frequency (RF) solver in the COMSOL multiphysics program (www.comsol.com). A typical computational domain (CD) is shown in **Figure 1d,** which shows a core-shell particle immersed in H_2O. The particle is illuminated with a uniform downward-directed plane wave with the E field polarized along the x-axis. The height of the CD is 1000 nm and perfectly matched layers (PMLs) (200 nm in height) are applied at the top and bottom of the domain to reduce backscatter from these boundaries. Perfect electric conductor (PEC) conditions are applied at the boundaries perpendicular to E, and perfect magnetic conductor (PMC) conditions are applied at the boundaries perpendicular to H. These symmetry boundary conditions (BCs) mimic the response of an infinite 2D array of coplanar identical nanoparticles with a center-to-center *x* and *y* lattice spacing equal to the spatial period P_x and P_y of the CD in the *x* and *y* directions, respectively. Thus, the field solution within the CD contains contributions from particles that exist outside the CD. The level of these contributions depends on the lattice spacing, i.e. the spatial period of the CD. In our analysis below, we determine values of P_x and P_y that are large enough so that the analysis accurately reflects the optical response of a single isolated colloidal particle. [3]. We use time-hamonic field theory to predict the spectral response of the particles, i.e. we solve

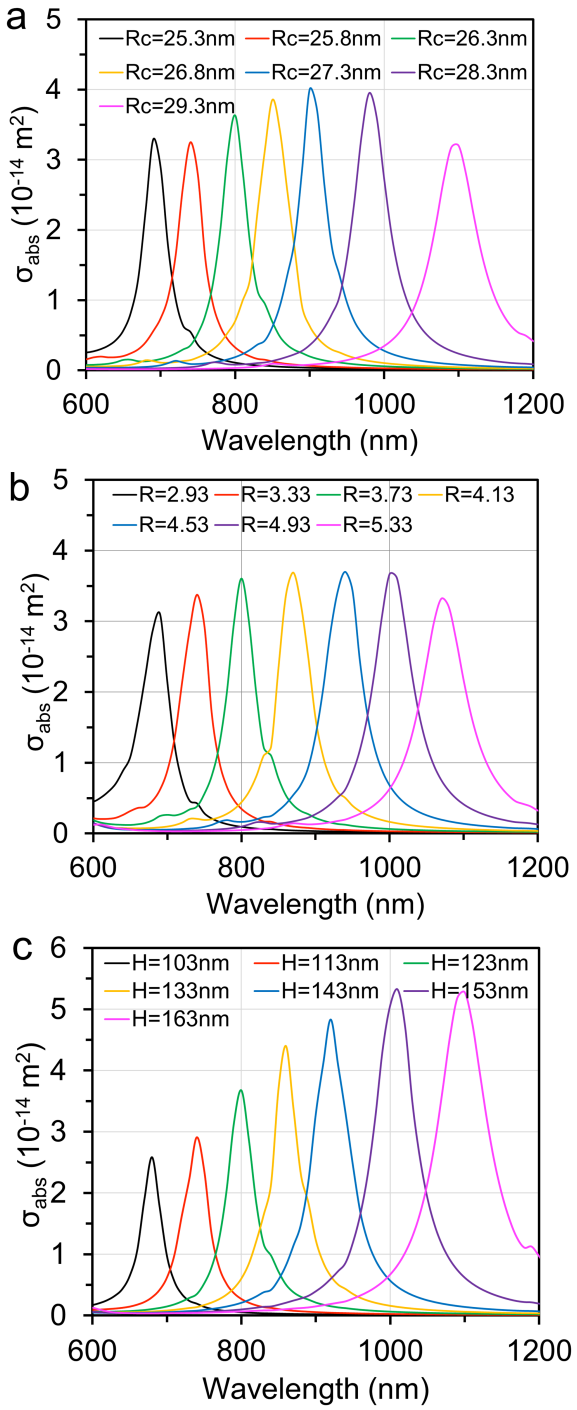

Figure 2. LSPR vs. nanostructure dimensions: (a) SiO_2@Au core-shell particles, (b) Au nanoframes and (c) Au nanorods.

$$\nabla\times\left(\mu_r^{-1}\nabla\times\mathbf{E}\right)-k_0^2\left(\varepsilon_r-\frac{\sigma}{\omega\varepsilon_0}\right)\mathbf{E}\quad 0$$

where μ_r, ε_r and σ are the relative permeability, permittivity and conductivity of the media, respectively.

3 LSPR VS. PARTICLE DIMENSIONS

We investigate the dependence of LSPR on the dimensional parameters of the three nanostructures. For the purpose of analysis, the particle volume is fixed at V_p = (50 nm)^3 for all particles. First, we explore the tunability of LSPR for the SiO_2@Au structure. In this analysis R_c is systematically increased from 25.3 nm to 29.3 nm (t_s decreases from 5.7 nm to 1.7 nm) and there is a corresponding shift in the LSPR wavelength in the NIR from 690 nm to 1100 nm as shown in **Figure 2a**. A similar analysis was performed for the nanocage. In this case *L* is fixed at 50 nm and the aspect ratio $R = L/W$ is increased from 2.93 to 5.33 (i.e. *W* decreases from 17 nm to 9.38 nm), which produces a redshift in the LSPR wavelength from 690 nm to 1070 nm as shown in **Figure 2b**. Lastly, for the Au nanorods, both the length *H* and radius R_d need to change in order to maintain a constant volume. As *H* increases from 103 nm to 163 nm (R_d decreases from 21.16 nm to 16.17 nm) and the LSPR peak red-shifts from 680 nm to 1110 nm as shown in **Figure 2c.**

The analysis shows that the LSPR of the three nanostructures with identical volumes can be readily tuned to the NIR by controlling their dimensions during synthesis. This NIR tunability is especially attractive for biomedical applications [4].

4 FIELD ENHANCEMENT

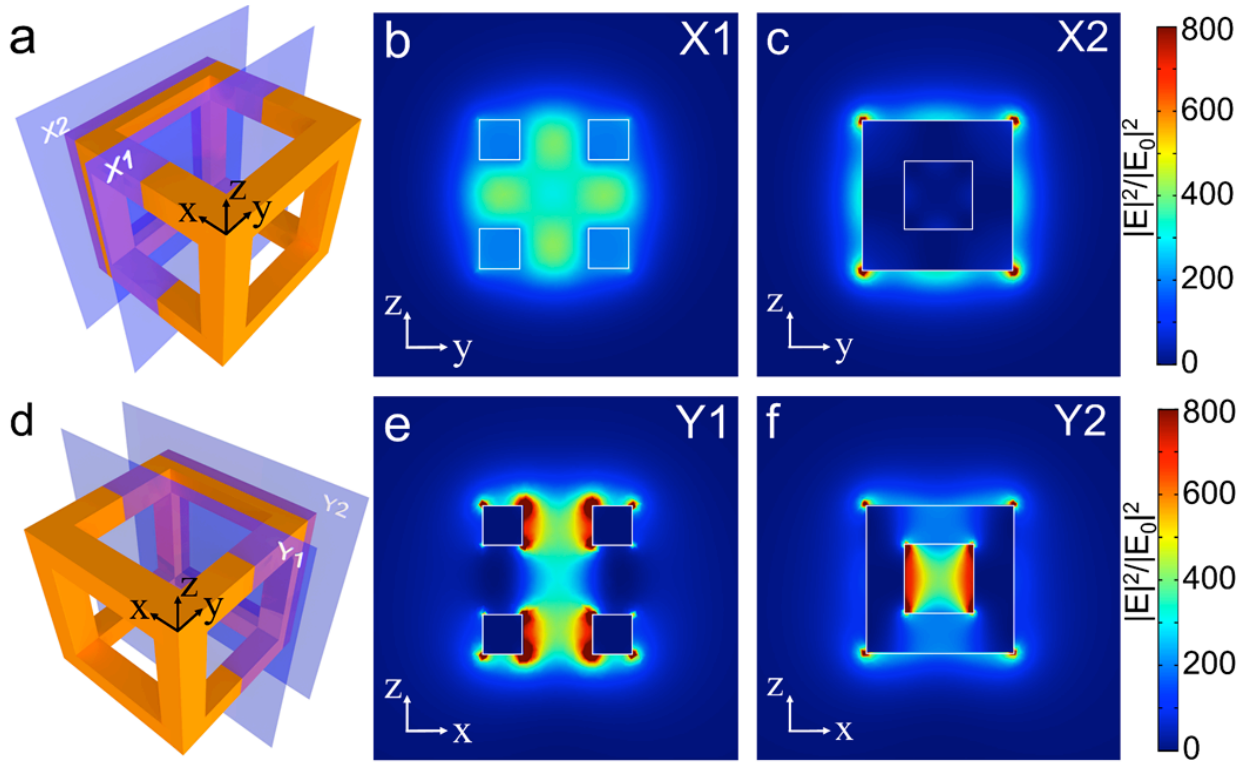

Figure 3. Local field enhancement profiles of the Au nanocage (L=50 nm and W=13.4 nm) at the LSPR wavelength of 800 nm: (a) and (d) are the conceptual schematics showing four designated planes. (b)-(c) and (e)-(f) show the profiles of LSPR-induced local field enhancement.

Next, we perform an optical analysis of three specific structures that have a LSPR wavelength of 800 nm: a SiO_2@Au core-shell particle with R_c=27.3 nm and t_s=3.7 nm, a nanocage with L=50 nm and W=13.4 nm and a nanorod with H=123 nm and R_d=19 nm. E field enhancement profiles for the Au nanocage are shown in **Figure 3.** Four planes are chosen to render the field plots. As shown in **Figure 3a**, two planes X1 and X2 are perpendicular to the polarization direction (x-axis). X1 overlaps the central symmetry plane and X2 cuts the middle of the nanowires that form the edge of the structure. **Figure 3b** shows a uniformly enhanced field intensity in X1 across the hollow interior of the nanocage. This region can potentially be loaded with theranostic agents that can be modulated by the enhanced field. **Figure 3c** illustrates several strongly enhanced hot spots at the outer surface of edge nanowires, which are primarily due to the dipolar resonance in those nanowires as they are aligned parallel to the polarization. Two additional planes Y1 and Y2 are defined perpendicular to the y-axis as illustrated in **Figure 3d**. Strong field enhancement profiles can be observed in the hollow interior of the Au nanocage in **Figures. 3e** and **3f**. This localized field concentration in the interior of the nanocage is attributed to the strong mode coupling between adjacent Au nanowire frame elements. The unique advantage of the nanocage over the core-shell particle is the abundance of coupled modes existing among the Au nanowires. The nanocage provides a larger number of hot spots on its surface that can be leveraged for theranostic applications. [5]

5 PHOTOTHERMAL ANALYSIS

The absorption cross-section depends on the magnitude and spatial extent of the LSPR-induced currents, which depend on the amount and the confiduration of the constituent gold. The current density and thermal power density (W/nm^3) distribution due to joule heating within the two particles is shown in **Figures 4a** and **4b**. The double headed red arrows in these figures show the direction of polarization. The small single headed red arrows represent the current density in the constituent gold. Note that the gold shell in the SiO_2@Au particle provides a continuous path for current to flow from one end of its induced dipole structure to the other. Consequently, it exhibits more uniform thermal dissipation over a relatively large volume of its Au shell. This is in contrast to the nanocage wherein only four nanowires, out of the twelve that form the nanoframe, carry significant current and produce heat. These four are aligned with the field polarization. The other eight nanowires in the frame are not aligned and have a negligible impact on optical absorption and heating when the particle has this orientation. Thus, even though the core-

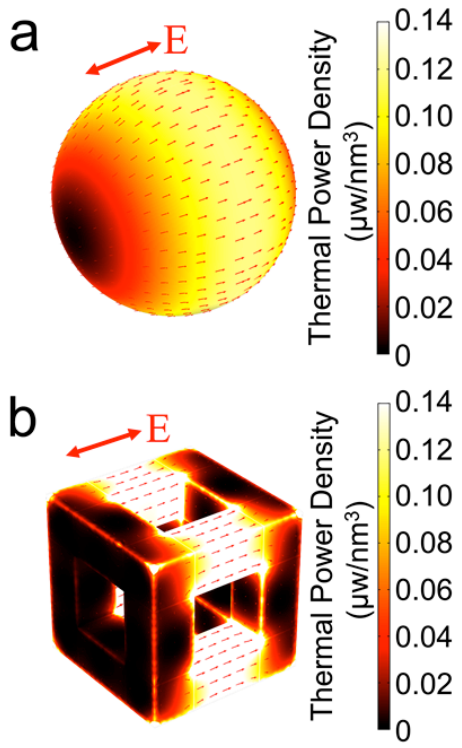

Figure 4. Spatial profiles of the thermal power density: (a) SiO_2@Au core-shell particle and (b) Au nanoframe. Small red arrows show the current density on the outer Au surfaces of two nanoparticles.

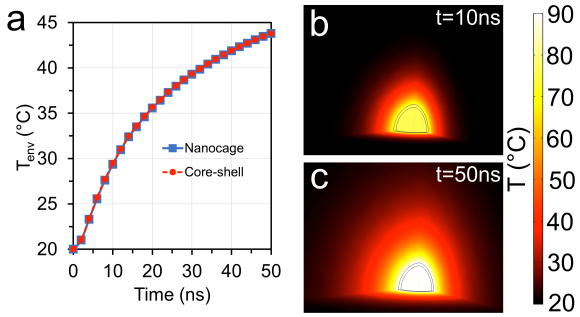

Figure 5. Transient temperature distribution of nanoparticles. (a) Time-dependent average temperature in proximity to the particles. (b)-(c) Temperature distribution due to the core-shell particle at (b) t=10 ns and (c) 50 ns.

shell particle contains less gold than the nanocage, this difference is offset because a higher percentage of the gold in the former contributes to heating, which renders the overall photothermal conversion efficiency of the two particles comparable. An additional factor that that may influence absorption includes the special optical cavity configuration of the core-shell particle, which can result in a stronger LSPR resonance than in the nanocage that has an open interior region.

We perform 3D thermodynamic analysis of these structures using coupled heat transfer and RF modules of the Comsol program. **Figure 5a** shows an identical change of the environmental temperature T_{env} for the core-shell (blue curve) and nanocage (red curve). T_{env} is calculated by averaging the temperature over a spherical surface of radius of 70 nm that is centered with respect to and surrounds the particles. The results indicate that T_{env} rises quickly from 20°C to 43°C within 50 ns which is consistent with typical laser pulse durations in photothermal therapy applications. **Figures 5b** and **5c** show the spatial profiles of the temperature for the SiO_2@Au core-shell at t=10 ns and 50 ns, respectively. The results imply a rapid exchange of thermal energy between the core-shell particle and the surrounding H_2O environment, causing a continuous rise of environmental temperature during 50 ns.

REFERENCES

[1] K. Liu, X. Xue, E. P. Furlani, Sci. Rep. 6, 34189 (2016).
[2] K. Liu, X. Xue, V. Sukhotskiy, E. P. Furlani, J. Phys. Chem. C 120, 27555 (2016).
[3] A. I. Henry, J. M. Bingham, E. Ringe, L. D. Marks, G. C. Schatz, R. P. J. Van Duyne, J. Phys. Chem. C 115, 9291 (2011).
[4] C. Ayala-Orozco; J. Liu, M. W. Knight, Y. Wang, J. K. Day, P. Nordlander, N. J. Halas, Nano Lett. 14, 2926 (2014).
[5] I. H. Karampelas, K. Liu, F. Alali, E. P. Furlani, J. Phys. Chem. C 120, 7256 (2016).